Nonlinear Dyn (2024) 112:6339–6356
https://doi.org/10.1007/s11071-024-09358-5

ORIGINAL PAPER

# Efficient time domain response computation of massive wave power farms

**Pol D. Spanos · Giovanni Malara · Felice Arena**

Received: 13 November 2023 / Accepted: 24 January 2024 / Published online: 1 March 2024


**Abstract** A potential future challenge in the wave energy sector will involve the design and construction of massive wave power farms. That is, collections of several ($> 100$) wave energy converters (WEC) operating in identical environmental conditions at a distance comparable with typical water wave lengths. In this context, the WECs are likely to be influenced by each another by radiation force effects that are associated with the radiated wave field propagated by WECs operating in the surrounding wave field. These effects are commonly captured by the Cummins' equation, where the radiation force is expressed as a convolution integral depending on the past values of the WEC response. Due to this mathematical representation, the time domain computation of the wave farm response can become computationally daunting. This article proposes one approach for computing efficiently the wave farm response in the time domain. Specifically, it demonstrates that the values of the radiation force components can be determined at each time step from their previous values by approximating the retardation function matrix elements via the Prony method. A notable advantage of this approach with respect to the ones available in the open literature is that it does not require either the storage of past response values or additional differential equations. Instead, it uses simple algebraic expressions for updating at each time instant the radiation force values. Obviously, this feature can induce significant computational efficiency in analyzing an actual wave farm facility.

The reliability and efficiency of the proposed algorithm are assessed vis-à-vis direct time domain comparisons and Monte Carlo data concerning a wave farm composed by an array of U-Oscillating Water Columns. Notably, the proposed methodology can be applied to any linear or nonlinear dynamics problem governed by differential equations involving memory effects.

**Keywords** Wave power farm · Array · Time-domain model · Fast numerical model

P. D. Spanos
L.B. Ryon Endowed Chair in Engineering, George R. Brown School of Engineering, MS 321, Rice University, Houston, TX 77005, USA
e-mail: spanos@rice.edu

G. Malara (✉) · F. Arena
Natural Ocean Engineering Laboratory (NOEL), "Mediterranea" University of Reggio Calabria, Loc. Feo di Vito, 89122 Reggio Calabria, Italy
e-mail: giovanni.malara@unirc.it

F. Arena
e-mail: arena@unirc.it

## 1 Introduction

The first technological developments of wave energy converters (WECs) focused on the determination of

working principles exploiting effectively the energy carried by water waves. This effort led to the development of a plethora of devices that, in most cases, did not proceed beyond small-scale modeling. Consequently, recent investigations have focused mainly on the analysis of a few types of WECs: single point absorbers [1]; and Oscillating Water Columns (OWCs) [2]. There are a few notable exceptions like the overtopping device [3], and they are the only ones with a clear potential for commercialization. Their key characteristics are: their reliability, since they can absorb a relevant fraction of incident wave energy and survive in harsh environmental conditions; and their flexibility, since they can be installed in a variety of locations, both nearshore and offshore, and thus be embedded in major infrastructures. In this light, certain studies have focused on the economic viability of these technologies, and on the determination of relevant economic indicators. Considering, for instance, the OWC case, estimates concerning plants installed in Portugal and Scotland have shown that the LCoE (Levelized Cost of Electricity) value ranges between 1.30 and 1.05 €/kWh [4]. This is a quite high value compared to the LCoE values of other renewables, such as concentrated solar (0.16 €/kWh) and offshore wind (0.10 €/kWh) [5]. To overcome this limitation, the concept of economic scaling has been considered as a means for reducing the unitary cost of WEC production, while increasing the overall power output of the wave farm. This concept has been investigated, for instance, in the wind energy sector, where the challenges associated with the large wind power were already assessed a decade ago [6].

Currently, wave farms are considered in few studies exploring problems of layout optimization of a specific WEC (see, for instance, Ref. [7–9]). However, in most cases, these analyses concern farms comprising a small number of WECs. This choice is frequently due to the significant computational cost associated with the inclusion of several WECs. Indeed, WEC dynamics and hydrodynamics is studied initially in the context of linear water wave theory, where effects due to diffraction and radiation of waves are taken into account. In this context, the computational complexity is twofold. Specifically, the determination of the hydrodynamic parameters can be cumbersome because of the complexity in the solution of the associated boundary value problems [10]. Further, the determination of the farm response in the time domain is quite challenging due to the fact that it must be computed by resorting to the Cummins' equation [11]. This equation accounts for hydrodynamic memory effects by convolution integrals. The first problem was addressed, for instance, by Sarkar [12] via a scheme involving multiple optimization strategies (statistical emulators, active learning, genetic algorithm). The second problem is largely unexplored. In this case, an efficient approach for determining the farm response is to work directly in the frequency domain, where the convolution integral reduces to the product of two frequency dependent functions via Fourier transform [13, 14]. However, this approach does not allow taking into consideration complex WEC dynamics behaviors due to large amplitude motions (see, for example, Ref. [15]), or nonlinear power take-off (PTO) effects [16]. Further, it does not allow testing PTO control strategies used in realistic applications. One approach for addressing some of these issues relies on the concept of statistical linearization [17]. This methodology has proved effective and efficient for determining the response and power output of OWC arrays [18, 19] as well as of single point absorbers [20], but it does not allow testing the performance of PTO controllers [21, 22]. Another approach considers the numerical integration of the equation of motion in the time domain after replacing the convolution integral by a computationally less costly operator. In this context, the typical approach involves introducing additional ordinary differential equations, so that additional fictitious degrees of freedom are utilized for capturing the hydrodynamic memory effects [23]. This is the state-space method. Otherwise, the convolution integral can be computed in the time domain within the numerical integration algorithm, with the proviso that the response past values are stored, and that at each time step the convolution integral values are updated. In this regard, useful instructions for increasing the computational efficiency of the procedure were given by Stavropoulou et al. [24]. Specifically, they emphasized that: a velocity-based formulation of the Cummins' equation should be preferred over the acceleration-based formulation, since the velocity is a (known) state of the system; the convolution integral can be computed over a fixed time interval to limit the number of stored past values; and integration by a fixed step solver should be preferred for reducing the uncertainties associated with the estimation of the response past values.

With their advantages notwithstanding, these alternatives for conducting a time domain integration possess features that may limit their application to the case of massive wave farms. Frequency domain approaches do not allow conducting a holistic WEC-PTO design, because the option of PTO control is ignored in the computation. State-space approaches require augmenting the number of differential equations under examination. Further, the identification of the parameters associated with the additional ordinary differential equations can be cumbersome. The direct numerical integration relying on storing the past velocity values becomes computationally prohibitive, unless resorting to parallel computing and a highly performance hardware configurations is adopted. However, even in this case, the execution of costly Monte Carlo simulations, where realizations of several samples of the response components must be determined, is challenging. Thus, approaches for computing efficiently the WEC farm response in realistic conditions are still quite desirable.

To address these limitations, herein a novel procedure for determining efficiently the response of massive wave power farms is developed. The procedure overcomes the limitations of the previously mentioned methods as it allows computing the radiation forces by updating the convolution integral values at each time step without storing past velocity values and without introducing additional differential equations. Instead, it utilizes simple algebraic expressions. To achieve this result, the procedure relies on the Prony method [25] for representing the kernels of the convolution integrals by superposition of damped harmonics. The particular mathematical form of the Prony approximation allows setting up conveniently a recurrence relation for updating the convolution integral values at each time step. In this regard, it is noted that the Prony method was already considered in other studies for representing analytically the kerned of the convolution integrals. For instance, Henriques et al. [26] used it for developing a nonlinear time—domain wave-to-wire model of the Mutriku OWC—breakwater; and Faedo et al. [27] used it for simulating linear multi-degree-of-freedom WECs. However, in the studies available in the open literature the method was formulated within the more traditional state-space approaches through the use of additional differential equations. In the following sections, it is shown that there is no need for augmenting the number of differential equations, and that a pair of algebraic expressions can be used for updating the convolution integral values at each time step. In the body of the paper, the fundamental equations for determining the farm response and the Prony method are first introduced. Then, the proposed numerical procedure is described. Finally, a numerical example concerning a U-Oscillating Water Column wave farm is utilized for assessing the reliability and the efficiency of the proposed approach of analysis.

## 2 Preliminary remarks on WEC dynamics and Prony method

This section describes the main equations used for determining the response of a wave farm, and the key equations involved in the Prony method.

Wave farm dynamics is governed by integro-differential equations arising from the formulation of the second Newton law in conjunction with the representation of the wave force via the Cummins' equations [10]. Under the assumption that the system exhibits nonlinear characteristics, the general formulation of a wave farm governing equation is

$$\boldsymbol{F}_{\mathrm{in}}(t) = \boldsymbol{F}_{\mathrm{e}}(t) - \int_{-\infty}^{t} \boldsymbol{K}(t-\tau)\dot{\boldsymbol{x}}(\tau)d\tau - \boldsymbol{F}_{s}(t) - \boldsymbol{F}_{\mathrm{d}}(t), \tag{1}$$

where $\boldsymbol{F}_{\mathrm{in}}(t)$ is the inertial force vector; $\boldsymbol{F}_{\mathrm{e}}(t)$ is the excitation force vector; $\boldsymbol{F}_{s}(t)$ is the restoring force vector; $\boldsymbol{F}_{\mathrm{d}}(t)$ is the dissipative force vector; $\boldsymbol{K}(t)$ denotes the retardation function matrix; $\boldsymbol{x}(t)$ is a vector comprising the individual WEC displacement values; and the dot above a symbol denotes differentiation with respect to time.

Specific representations of the forces are derived based on the configuration and working principle of the WECs. However, it is generally recognized that inertial forces $\boldsymbol{F}_{in}(t)$ must include the so-called infinite frequency added mass matrix $\boldsymbol{M}^{add}(\infty)$ (as a consequence of the Cummins' equation). This is a fully populated matrix accounting for water-related inertial effects on the WECs. Further, the convolution integral is used for expressing the radiation force that is the force due to the wave field changes induced exclusively by the WEC dynamics. The excitation force $\boldsymbol{F}_{\mathrm{e}}(t)$ is determined by solving the associated

diffraction water wave problem. This problem is posed by assuming that the WECs are held fixed during their interaction with the incident waves, and includes the incident wave field characteristics. The symbols $\boldsymbol{M}^{add}(\infty)$, $\boldsymbol{K}(t)$, and $\boldsymbol{F}_e(t)$ denote geometrically dependent functions of the wave farm, which are computed by standard numerical codes such as WAMIT [28] and NEMOH [29]; by utilizing the boundary element method for solving the radiation and diffraction water wave problems; or by analytical methods [30].

In the next section, the Prony method is used for representing efficiently the radiation force. Specifically, the method is used to approximate each element of the retardation function matrix $K_{ij}(t)$ by superposition of damped harmonics of the form

$$K_{ij}(t) = \sum_{m=1}^{+\infty} \beta_{ijm} e^{-\alpha_{ijm} t} \cos\left(\omega_{ijm} t + \phi_{ijm}\right), \tag{2}$$

in which $\beta_{ijm}$, $\alpha_{ijm}$, $\omega_{ijm}$, and $\phi_{ijm}$ are parameters identified from the known retardation function. After selecting the order of the approximation of the Prony expansion $M$, various identification procedures are available in the open literature, such as Classic Prony, Prony, Pisarenko, Linear predictor, and Modified Prony [31]. In wave energy applications, the approach described by Roessling and Ringwood [32] can be used to identify the parameters. Note that the particular mathematical form of the Prony approximation is critical for the development of the proposed approach of dynamic analysis in the ensuing section.

## 3 Efficient computation of the WEC response in time domain

This section describes the numerical algorithm for solving the integro-differential Eq. (1) without the storage of past velocity values or the use of additional differential equations. Initially, the numerical procedure for computing the convolution integrals is derived. Then, a numerical algorithm based on the use of the incremental form of the equation of motion is derived in conjunction with the proposed numerical approach. A flowchart elucidating the procedure for producing a related numerical code is given.

### 3.1 Radiation force treatment

Consider the radiation force in Eq. (1) pertaining to a wave farm whose dynamics involves $N$ degrees of freedom. Then, assume that each element of the retardation function matrix $\boldsymbol{K}(t)$ can be represented via the Prony expansion shown in Eq. (2). In this context, the elements of the radiation force vector,

$$\boldsymbol{I}(t) = \int_{-\infty}^{t} \boldsymbol{K}(t-\tau)\dot{\boldsymbol{x}}(\tau)d\tau, \tag{3}$$

can be computed using the equation,

$$I_i(t) = \int_{-\infty}^{t} \sum_{j=1}^{N} \sum_{m=1}^{+\infty} \beta_{ijm} e^{-\alpha_{ijm}(t-\tau)} \cos\left[\omega_{ijm}(t-\tau) + \phi_{ijm}\right] \dot{x}_j(\tau)d\tau, for i = 1, \ldots, N. \tag{4}$$

It can be rewritten in compact notation as,

$$I_i(t) = \sum_{m=1}^{+\infty} I_{im}^{c}(t), \tag{5}$$

where

$$I_{im}^{c}(t) = \int_{-\infty}^{t} \sum_{j=1}^{N} \beta_{ijm} e^{-\alpha_{ijm}(t-\tau)} \cos\left[\omega_{ijm}(t-\tau) + \phi_{ijm}\right] \dot{x}_j(\tau)d\tau. \tag{6}$$

Next, introduce the auxiliary function

$$\tilde{I}_i(t) = \int_{-\infty}^{t} \sum_{j=1}^{N} \sum_{m=1}^{+\infty} \beta_{ijm} e^{-\alpha_{ijm}(t-\tau)} \sin\left[\omega_{ijm}(t-\tau) + \phi_{ijm}\right] \dot{x}_j(\tau)d\tau, for i = 1, \ldots, N, \tag{7}$$

which is obtained by replacing the cosine function by a sine function in Eq. (4), and, similarly, recast it in the compact form,

$$\tilde{I}_i(t) = \sum_{m=1}^{+\infty} I_{im}^{s}(t), \tag{8}$$

in which,

$$I_{im}^{s}(t) = \int_{-\infty}^{t} \sum_{j=1}^{N} \beta_{ijm} e^{-\alpha_{ijm}(t-\tau)} \sin\left[\omega_{ijm}(t-\tau) + \phi_{ijm}\right] \dot{x}_j(\tau)d\tau. \tag{9}$$

Then, eqs. (4) and (7) are computed at a time instant $t+\Delta t$ and the computation of the integrals is split in the intervals $(-\infty, t)$ and $[t, t+\Delta t]$. That is,

$$\begin{aligned} I_i(t+\Delta t) &= \int_{-\infty}^{t+\Delta t} \sum_{j=1}^{N} \sum_{m=1}^{+\infty} \beta_{ijm} e^{-\alpha_{ijm}(t+\Delta t-\tau)} \\ &\quad \cos\left[\omega_{ijm}(t+\Delta t-\tau)+\phi_{ijm}\right]\dot{x}_j(\tau)d\tau \\ &= \int_{-\infty}^{t} \sum_{j=1}^{N} \sum_{m=1}^{+\infty} \beta_{ijm} e^{-\alpha_{ijm}(t+\Delta t-\tau)} \\ &\quad \cos\left[\omega_{ijm}(t+\Delta t-\tau)+\phi_{ijm}\right]\dot{x}_j(\tau)d\tau \\ &\quad + \int_{t}^{t+\Delta t} \sum_{j=1}^{N} \sum_{m=1}^{+\infty} \beta_{ijm} e^{-\alpha_{ijm}(t+\Delta t-\tau)} \\ &\quad \cos\left[\omega_{ijm}(t+\Delta t-\tau)+\phi_{ijm}\right]\dot{x}_j(\tau)d\tau, \end{aligned} \tag{10}$$

and

$$\begin{aligned} \tilde{I}_i(t+\Delta t) &= \int_{-\infty}^{t+\Delta t} \sum_{j=1}^{N} \sum_{m=1}^{+\infty} \beta_{ijm} e^{-\alpha_{ijm}(t+\Delta t-\tau)} \\ &\quad \sin\left[\omega_{ijm}(t+\Delta t-\tau)+\phi_{ijm}\right]\dot{x}_j(\tau)d\tau \\ &= \int_{-\infty}^{t} \sum_{j=1}^{N} \sum_{m=1}^{+\infty} \beta_{ijm} e^{-\alpha_{ijm}(t+\Delta t-\tau)} \\ &\quad \sin\left[\omega_{ijm}(t+\Delta t-\tau)+\phi_{ijm}\right]\dot{x}_j(\tau)d\tau \\ &\quad + \int_{t}^{t+\Delta t} \sum_{j=1}^{N} \sum_{m=1}^{+\infty} \beta_{ijm} e^{-\alpha_{ijm}(t+\Delta t-\tau)} \\ &\quad \sin\left[\omega_{ijm}(t+\Delta t-\tau)+\phi_{ijm}\right]\dot{x}_j(\tau)d\tau. \end{aligned} \tag{11}$$

Further, the integrals defined over the time interval $[t, t+\Delta t]$ can be approximated numerically by the trapezoidal rule. Thus, eqs. (10) and (11) can be rewritten equivalently as

$$\begin{aligned} I_i(t+\Delta t) &= \sum_{j=1}^{N} \sum_{m=1}^{+\infty} e^{-\alpha_{ijm}\Delta t}\cos\left(\omega_{ijm}\Delta t\right) I^c_{im}(t) \\ &\quad - e^{-\alpha_{ijm}\Delta t}\sin\left(\omega_{ijm}\Delta t\right) I^s_{im}(t) \\ &\quad + \frac{1}{2}\beta_{ijm}\Delta t\{\cos\left(\phi_{ijm}\right)\Delta\dot{x}_j(t+\Delta t) \\ &\quad + \left[e^{-\alpha_{ijm}\Delta t}\cos\left(\omega_{ijm}\Delta t+\phi_{ijm}\right)+\cos\left(\phi_{ijm}\right)\right]\dot{x}_j(t)\}, \end{aligned} \tag{12}$$

and

$$\begin{aligned} \tilde{I}_i(t+\Delta t) &= \sum_{j=1}^{N} \sum_{m=1}^{+\infty} e^{-\alpha_{ijm}\Delta t}\cos\left(\omega_{ijm}\Delta t\right) I^s_{im}(t) \\ &\quad + e^{-\alpha_{ijm}\Delta t}\sin\left(\omega_{ijm}\Delta t\right) I^c_{im}(t) \\ &\quad + \frac{1}{2}\beta_{ijm}\Delta t\{\sin\left(\phi_{ijm}\right)\Delta\dot{x}_j(t+\Delta t) \\ &\quad + \left[e^{-\alpha_{ijm}\Delta t}\sin\left(\omega_{ijm}\Delta t+\phi_{ijm}\right)+\sin\left(\phi_{ijm}\right)\right]\dot{x}_j(t)\}, \end{aligned} \tag{13}$$

where

$$\Delta\dot{x}_j(t+dt) = \dot{x}_j(t+\Delta t) - \dot{x}_j(t) \tag{14}$$

is the velocity increment from $t$ to $t+\Delta t$. A comparison between eqs. (12), (13), and (5–8) shows that,

$$\begin{aligned} I^c_{im}(t+\Delta t) &= \sum_{j=1}^{N} e^{-\alpha_{ijm}\Delta t}\cos\left(\omega_{ijm}\Delta t\right) I^c_{im}(t) \\ &\quad - e^{-\alpha_{ijm}\Delta t}\sin\left(\omega_{ijm}\Delta t\right) I^s_{im}(t) \\ &\quad + \frac{1}{2}\beta_{ijm}\Delta t\{\cos\left(\phi_{ijm}\right)\Delta\dot{x}_j(t+\Delta t) \\ &\quad + \left[e^{-\alpha_{ijm}\Delta t}\cos\left(\omega_{ijm}\Delta t+\phi_{ijm}\right)+\cos\left(\phi_{ijm}\right)\right]\dot{x}_j(t)\}, \end{aligned} \tag{15}$$

and

$$\begin{aligned} I^s_{im}(t+\Delta t) &= \sum_{j=1}^{N} e^{-\alpha_{ijm}\Delta t}\cos\left(\omega_{ijm}\Delta t\right) I^s_{im}(t) \\ &\quad + e^{-\alpha_{ijm}\Delta t}\sin\left(\omega_{ijm}\Delta t\right) I^c_{im}(t) \\ &\quad + \frac{1}{2}\beta_{ijm}\Delta t\{\sin\left(\phi_{ijm}\right)\Delta\dot{x}_j(t+\Delta t) \\ &\quad + \left[e^{-\alpha_{ijm}\Delta t}\sin\left(\omega_{ijm}\Delta t+\phi_{ijm}\right)+\sin\left(\phi_{ijm}\right)\right]\dot{x}_j(t)\}. \end{aligned} \tag{16}$$

Clearly, these expressions show that, given the values of $I^c_{im}(t)$ and $I^s_{im}(t)$, which are known at a given time $t$, the numerical computation of the radiation force at time $t+\Delta t$ is obtained via an algebraic expression dependent on the current velocity values $\dot{x}_j(t)$ and on the forward velocity values $\dot{x}_j(t+\Delta t)$. Note that the computation of the radiation force requires only the computation of $I_{im}(t+dt)$ (see Eq. 5), but the auxiliary function (7) is necessary for formulating a numerical procedure avoiding the need of storing the past velocity values through the simultaneous update of the $I^c_{im}(t)$ and $I^s_{im}(t)$ values. Further, note that eqs. (12) and (13) require the knowledge of the increment $\Delta\dot{x}_j(t+\Delta t)$, which is determined within the algorithm used for conducting the numerical integration of the equation of motion.

### 3.2 Numerical integration of the equation of motion

To conduct the step-by-step analysis of a wave farm, the incremental equation of motion can be used. Specifically, considering the time instants $t_l$ and $t_{l+1} = t_l + \Delta t$, the difference between the vector equilibrium relationships (1) at those time instants is:

$$\Delta \boldsymbol{F}_{\text{in}} = \Delta \boldsymbol{F}_{\text{e}} - \Delta \boldsymbol{I} + \Delta \boldsymbol{F}_s + \Delta \boldsymbol{F}_{\text{d}}, \tag{17}$$

where

$$\Delta \boldsymbol{I} = \boldsymbol{I}(t_{l+1}) - \boldsymbol{I}(t_l). \tag{18}$$

The force vector increments in Eq. (17) are generally dependent on the specific WEC considered. Nevertheless, commonly they are of the form

$$\Delta \boldsymbol{F}_{\text{in}} = \boldsymbol{F}_{\text{in}}(t_{l+1}) - \boldsymbol{F}_{\text{in}}(t_l) = \boldsymbol{M}_0 \Delta \boldsymbol{x}, \tag{19}$$

$$\Delta \boldsymbol{F}_{\text{d}} = \boldsymbol{F}_{\text{d}}(t_{l+1}) - \boldsymbol{F}_{\text{d}}(t_l) = \boldsymbol{C}_0 \Delta \dot{\boldsymbol{x}}, \tag{20}$$

$$\Delta \boldsymbol{F}_s = \boldsymbol{F}_s(t_{l+1}) - \boldsymbol{F}_s(t_l) = \boldsymbol{K}_0 \Delta \boldsymbol{x}, \tag{21}$$

and

$$\Delta \boldsymbol{F}_{\text{e}} = \boldsymbol{F}_{\text{e}}(t_{l+1}) - \boldsymbol{F}_{\text{e}}(t_l). \tag{22}$$

In the preceding equations, the displacements, velocities, and accelerations increments are given by the equations

$$\Delta \boldsymbol{x} = \boldsymbol{x}_{l+1} - \boldsymbol{x}_l, \tag{23}$$

$$\Delta \dot{\boldsymbol{x}} = \dot{\boldsymbol{x}}_{l+1} - \dot{\boldsymbol{x}}_l, \tag{24}$$

and

$$\Delta \ddot{\boldsymbol{x}} = \ddot{\boldsymbol{x}}_{l+1} - \ddot{\boldsymbol{x}}_l, \tag{25}$$

with $\boldsymbol{M}_0$, $\boldsymbol{C}_0$ and $\boldsymbol{K}_0$ denoting mass, damping, and stiffness matrices, whose elements are influence coefficients. In the case of linear force vectors, these are classical mass, damping, and stiffness values, but in the case of nonlinear force vectors, these are time dependent values computed by a Taylor expansion of the nonlinear force vector at the initial time instant $t_l$. For instance, if the restoring and damping forces are nonlinear and depend on displacements and velocities, respectively, the influence coefficients are [33]

$$\{\boldsymbol{K}_0\}_{ij} = \left.\frac{d\boldsymbol{F}_{s,i}}{d\boldsymbol{x}_j}\right|_t, \tag{26}$$

and

$$\{\boldsymbol{C}_0\}_{ij} = \left.\frac{d\boldsymbol{F}_{d,i}}{d\dot{\boldsymbol{x}}_j}\right|_t. \tag{27}$$

Thus, the incremental equation of motion becomes

$$\boldsymbol{M}_0 \Delta \boldsymbol{x} + \boldsymbol{C}_0 \Delta \dot{\boldsymbol{x}} + \Delta \boldsymbol{I} + \boldsymbol{K}_0 \Delta \boldsymbol{x} = \Delta \boldsymbol{F}_e. \tag{28}$$

Substituting the values of the convolution integrals given in eqs. (5) and (12), Eq. (28) becomes,

$$\boldsymbol{M}_0 \Delta \boldsymbol{x} + [\boldsymbol{C}_0 + \boldsymbol{C}_{\Delta I}] \Delta \dot{\boldsymbol{x}} + \boldsymbol{K}_0 \Delta \boldsymbol{x} = \Delta \boldsymbol{F}_e - \boldsymbol{F}_{\Delta I}, \tag{29}$$

where $\boldsymbol{C}_{\Delta I}$ is a matrix with elements

$$\{\boldsymbol{C}_{\Delta I}\}_{ij} = \sum_{m=1}^{+\infty} \frac{1}{2} \beta_{ijm} \Delta t \cos\left(\phi_{ijm}\right), \text{ for } i,j = 1,\ldots,N, \tag{30}$$

and $\boldsymbol{F}_{\Delta I}$ is a force vector with elements

$$\begin{aligned} \{\boldsymbol{F}_{\Delta I}\}_i = \sum_{j=1}^{N} \sum_{m=1}^{+\infty} & \left[e^{-\alpha_{ijm}\Delta t} \cos\left(\omega_{ijm}\Delta t\right) - 1\right] I_{im}^c(t_l) \\ & - e^{-\alpha_{ijm}\Delta t} \sin\left(\omega_{ijm}\Delta t\right) I_{im}^s(t_l) \\ & + \frac{1}{2} \beta_{ijm} \Delta t \left[e^{-\alpha_{ijm}\Delta t} \cos\left(\omega_{ijm}\Delta t + \phi_{ijm}\right) \right. \\ & \left. + \cos\left(\phi_{ijm}\right)\right] \dot{x}_j(t_l), \text{ for } i = 1,\ldots,N. \end{aligned} \tag{31}$$

Equation (29) is the incremental form of the equation of motion (1) which accounts for the radiation force vector by an additional damping term $\boldsymbol{C}_{\Delta I}$ depending on the Prony parameters $\beta_{ijm}$ and $\phi_{ijm}$; and by an external force vector accounting for the actual external force increment, and for the current values of the radiation force via the terms $I_{im}^c(t_l)$ and $I_{im}^s(t_l)$.

Equation (29) is integrated numerically by establishing initially the relation between displacement, velocity, and acceleration, and then, determining the value of the displacement increment. For instance, by utilizing the constant average acceleration method (see Ref. [33]), the displacement increment is calculated by the equation

$$\tilde{\boldsymbol{K}} \cdot \Delta \boldsymbol{x} = \Delta \tilde{\boldsymbol{F}}, \tag{32}$$

where

$$\tilde{\boldsymbol{K}} = \boldsymbol{K}_0 + \frac{2}{\Delta t}(\boldsymbol{C}_0 + \boldsymbol{C}_{\Delta I}) + \frac{4}{\Delta t^2} \boldsymbol{M}_0, \tag{33}$$

and

$$\Delta\tilde{\boldsymbol{F}} = \Delta\boldsymbol{F}_{\mathrm{e}} - \boldsymbol{F}_{\Delta I} + 2(\boldsymbol{C}_0 + \boldsymbol{C}_{\Delta I}) \cdot \dot{\boldsymbol{x}}_l + \boldsymbol{M} \cdot \left[\frac{4}{\Delta t}\dot{\boldsymbol{x}}_l + 2\ddot{\boldsymbol{x}}_l\right], \tag{34}$$

with WEC accelerations readily determinable directly from the equation of motion. That is,

$$\ddot{\boldsymbol{x}}_l = \boldsymbol{M}^{-1} \cdot [\boldsymbol{F}_{\mathrm{e}} - \boldsymbol{I}(t_l) + \boldsymbol{F}_{\mathrm{d}} + \boldsymbol{F}_s], \tag{35}$$

and the velocity increment is determined by the equation

$$\Delta\dot{\boldsymbol{x}} = \frac{2}{\Delta t}\Delta\boldsymbol{x} - 2\dot{\boldsymbol{x}}_l. \tag{36}$$

The mechanization of the proposed approach is captured in Fig. 1. The flowchart points out the fact that the effect of the radiation force is incorporated via the vector force $\boldsymbol{I}(t)$, which is determined at each time instant via the updated values of the $I^c_{im}(t)$ terms. The procedure can be utilized also in the case of nonlinear wave farm models with the stipulation that the values of $\boldsymbol{K}_0$ and $\boldsymbol{C}_0$ are updated at each time instant consistently with eqs. (26–27).

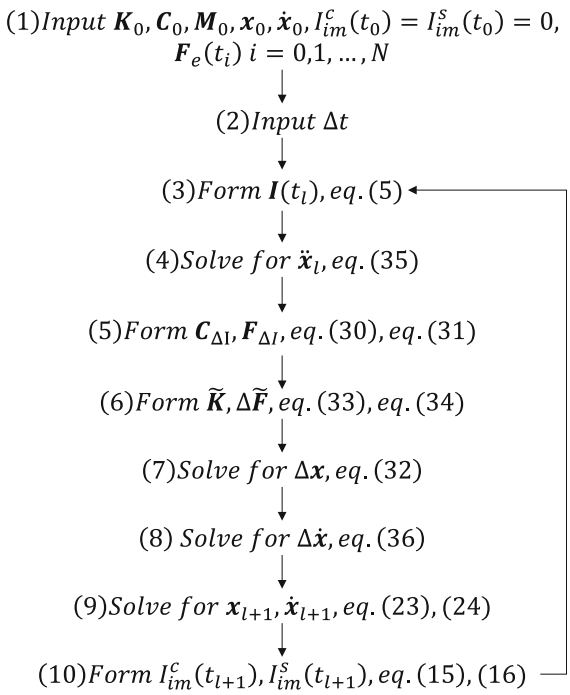


**Fig. 1** Flowchart for implementing the proposed numerical procedure

## 4 Numerical examples

To elucidate the details about the application of the proposed method, a preliminary numerical example regarding a classical nonlinear single-degree-of-freedom (SDOF) oscillator comprising a linear-plus-cubic stiffness and with memory effects is discussed. Next, the proposed approach is used by a case study regarding a farm comprising an array of U-Oscillating Water Column (U-OWC) energy harvesters. U-OWCs are wave energy converters exploiting the sea wave energy by the typical OWC working principle. Thus, they comprise a water column excited by the external wave field that compresses and expands an air pocket located above it. The chamber enclosing the air pocket is connected to the atmosphere by a small orifice in which an air turbine is installed. The alternating compression/expansion of the air pocket creates an air flow through the orifice that drives the air turbine, thus producing electrical energy. Compared to classical OWC systems, this device includes also a small vertical U-shaped duct connecting the water column to the open wave field. This case study has been selected as U-OWCs are one of the few devices that have reached the prototype scale stage. Further, it is one of the few that have the potential for being implemented in the form of a massive wave farm. The fact that they are commonly embedded in vertical breakwaters, whose layout may span several hundred meters, makes it quite likely to be installed as a wave farm. In this regard, it is worth mentioning the farm built in Civitavecchia (Rome, Italy), where a plant comprising more than 100 converters has been constructed [34].

**Table 1** Parameters of the Prony expansion used for representing the Kernel of convolution integral of Eq. (37)

| $n$ | 1 | 2 | 3 |
|---|---|---|---|
| $\alpha_n$ | 0.83 | 0.93 | 1.15 |
| $\beta_n$ | 2.52 | 0.77 | 3.19 |
| $\omega_n$ | 1.18 | 3.67 | 2.59 |
| $\phi_n$ | 1.18 | − 2.80 | − 0.63 |

### 4.1 Response of a nonlinear SDOF oscillator with memory effects

The application of the proposed method is first elucidated by a numerical example involving a SDOF oscillator governed by the equation of motion

$$m\ddot{x}+c\dot{x}+kx+\varepsilon x^3+\int_{-\infty}^{t} K(t-\tau)\dot{x}(\tau)d\tau = F(t), \tag{37}$$

with parameters $m = 2.21$, $c = 0.50$, $k = 1.0$, and $\varepsilon = 0.25$. The kernel of the convolution integral is represented by a Prony expansion involving three parameters whose values are shown in Table 1. The excitation of the system is sinusoidal with amplitude $|F| = 0.83$ and period $T = 4.26$.

Following the procedure described in Sect. 3.2, Eq. (37) is taken in incremental form. That is,

$$m\Delta\ddot{x}+c\Delta\dot{x}+k_i\Delta x+\Delta I = \Delta F, \tag{38}$$

where the stiffness value $k_i$ is computed at each time step by utilizing the initial displacement value $x_i$ through the equation

$$k_i = k+3\varepsilon x_i^2. \tag{39}$$

This is done consistently with the typical application of the step-by-step integration methods [33] (see also Eq. 26). The procedure described in Sect. 3.1 allows recasting the convolution integral increment in the form

$$\begin{aligned}\Delta I =& I(t+\Delta t)-I(t)\\ =&\sum_{n=1}^{3}\left[e^{-\alpha_n\Delta t}\cos(\omega_n t+\phi_n)-1\right]I_n^c(t)\\ &-e^{-\alpha_n\Delta t}\sin(\omega_n t+\phi_n)I_n^s(t)\\ &+\frac{1}{2}\beta_n\Delta t\left\{\cos\phi_n\Delta\dot{x}+\left[\cos\phi_n+e^{-\alpha_n\Delta t}\cos(\omega_n\Delta t+\phi_n)\right]\dot{x}(t)\right\},\end{aligned} \tag{40}$$

in which the quantities $I_n^c(t)$ and $I_n^s(t)$ are known values at each time step. In this regard, note that they are defined by the equations

$$I_n^c(t) = \int_{-\infty}^{t}\beta_n e^{-\alpha_n(t-\tau)}\cos[\omega_n(t-\tau)+\phi_n]\dot{x}(\tau)d\tau, \tag{41}$$

and

$$I_n^s(t) = \int_{-\infty}^{t}\beta_n e^{-\alpha_n(t-\tau)}\sin[\omega_n(t-\tau)+\phi_n]\dot{x}(\tau)d\tau. \tag{42}$$

However, their numerical values within the numerical scheme are determined by updating their values known at the previous time instant. This is done by using the counterpart of the auxiliary Eq. (13) for the SDOF case, which is captured by the equation

$$\begin{aligned}\tilde{I}(t+\Delta t) =&\sum_{n=1}^{3} e^{-\alpha_n\Delta t}\cos(\omega_n\Delta t)I_n^s(t)\\ &+e^{-\alpha_n\Delta t}\sin(\omega_n\Delta t)I_n^c(t)\\ &+\frac{1}{2}\beta_n\Delta t\{\sin(\phi_n)\Delta\dot{x}\\ &+\left[e^{-\alpha_n\Delta t}\sin(\omega_n\Delta t+\phi_n)+\sin(\phi_n)\right]\dot{x}(t)\}.\end{aligned} \tag{43}$$

This leads to the equations

$$\begin{aligned}I_n^c(t+\Delta t) =&e^{-\alpha_n\Delta t}\cos(\omega_n\Delta t)I_n^c(t)-e^{-\alpha_n\Delta t}\sin(\omega_n\Delta t)I_n^s(t)\\ &+\frac{1}{2}\beta_n\Delta t\{\cos(\phi_n)\Delta\dot{x}\\ &+\left[e^{-\alpha_n\Delta t}\cos(\omega_n\Delta t+\phi_n)+\cos(\phi_n)\right]\dot{x}(t)\},\end{aligned} \tag{44}$$

and

$$\begin{aligned}I_n^s(t+\Delta t) =&e^{-\alpha_n\Delta t}\cos(\omega_n\Delta t)I_n^s(t)\\ &+e^{-\alpha_n\Delta t}\sin(\omega_n\Delta t)I_n^c(t)\\ &+\frac{1}{2}\beta_n\Delta t\{\sin(\phi_n)\Delta\dot{x}\\ &+\left[e^{-\alpha_n\Delta t}\sin(\omega_n\Delta t+\phi_n)+\sin(\phi_n)\right]\dot{x}(t)\}.\end{aligned} \tag{45}$$

Finally, substituting Eq. (40) into (38), and after a few algebraic manipulations, the incremental equation of motion

$$\begin{aligned}&m\Delta x+\left(c+\sum_{n=1}^{3}\frac{1}{2}\beta_n\Delta t\cos\phi_n\right)\Delta\dot{x}+k_i\Delta x\\ =&\Delta F-\sum_{n=1}^{3}\left[e^{-\alpha_n\Delta t}\cos(\omega_n t+\phi_n)-1\right]I_n^c(t)\\ &-e^{-\alpha_n\Delta t}\sin(\omega_n t+\phi_n)I_n^s(t)\\ &+\frac{1}{2}\beta_n\Delta t\left[\cos\phi_n+e^{-\alpha_n\Delta t}\cos(\omega_n\Delta t+\phi_n)\right]\dot{x}(t),\end{aligned} \tag{46}$$

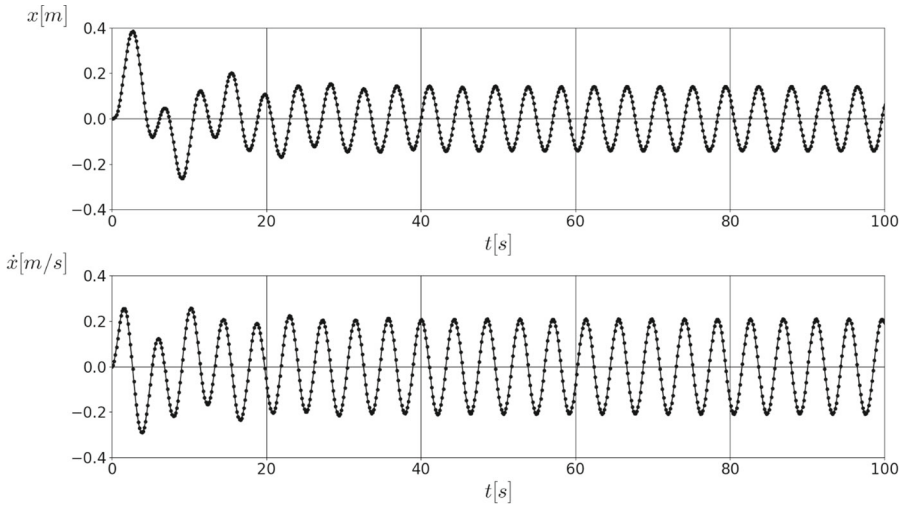


**Fig. 2** Response of a nonlinear SDOF with memory to sinusoidal excitation. Continuous line: computation by classical trapezoidal integration. Circles: integration by Prony approximation

is obtained, which is recognized as the counterpart of Eq. (29) in the case of SDOF systems.

The response of this system is computed over a time span of 100 s with a constant time step $\Delta t = 0.01$ s from quiescent initial conditions, and by setting the initial values of $I_n^c(0) = I_n^s(0) = 0$. The system acceleration between two successive time instants is considered constant. Therefore, the expressions of the constant average acceleration method can be used for computing the effective stiffness and effective load. The response obtained by the proposed method is shown in Fig. 2 (circles) and is compared with data obtained by applying the classical trapezoidal integration for the computation of the memory term (continuous line). In this regard, note that the kernel function used in the standard computational scheme is obtained by Eq. (2) over a time windows of 10 s with the same time step $\Delta t$ used in the numerical integration. The figure shows a perfect agreement between the proposed approximation and the standard approach available in the literature. Notably, the system response is well captured in both their transient and steady state parts.

### 4.2 Case study: U-oscillating water column wave power farm

Next, the case study concerning a U-OWC plant installed in the Port of Salerno (Italy) is considered [35]. While the studies concerning the design and construction of the plant started about a decade ago, the whole infrastructure has been completed only recently with the installation of three vertical breakwaters comprising totally 30 independent U-OWC harvesters, thus making it the most recent case study on U-OWC wave energy converters.

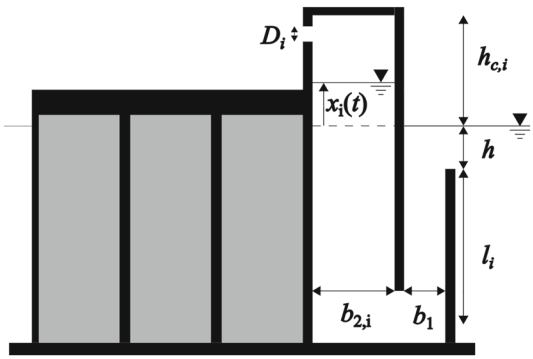


**Fig. 3** Vertical cross section of a U-OWC wave energy converter

The typical cross section and plant view of a U-OWC plant are shown in Figs. 3 and 4, where the main geometrical parameters used in the U-OWC numerical model are shown. The numerical data regarding the Salerno case study are shown in Table 2 and are utilized for producing the numerical results shown in the next sections. In this regard, note that the table shows the installation water depth $d$, as well. To simulate the behavior of a wave farm, the U-OWC chambers are supposed to be geometrically identical. However, the proposed method can be implemented, as well, in the case of chambers having different sizes.

Prior to computing the system response, the hydrodynamic parameters associated with the U-OWC wave

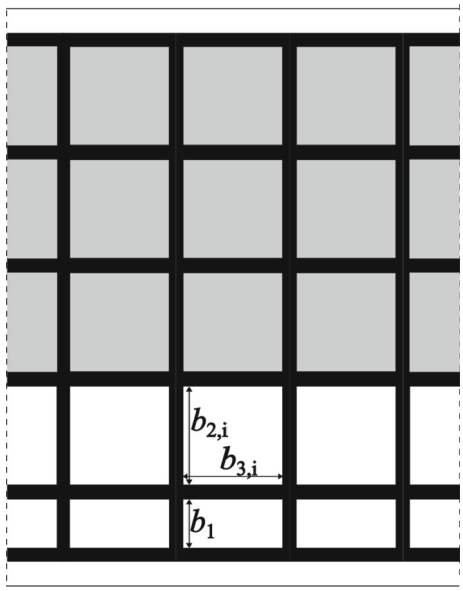


**Fig. 4** Horizontal cross section of a vertical breakwater caisson embedding a U-OWC array

**Table 2** Geometrical parameters of the U-OWC chambers and water depth $d$

| | |
|---|---|
| $b_1$ (m) | 2.0 |
| $b_{2,i}$ (m) | 4.0 |
| $b_{3,i}$ (m) | 4.0 |
| $l_i$ (m) | 5.65 |
| $h_{c,i}$ (m) | 5.6 |
| $D_i$ (m) | 0.75 |
| $d$ (m) | 12.0 |

farm must be determined. For this purpose, the semi-analytical solution developed by Malara and Arena [36] is used. It allows determining the system excitation vector, infinite frequency added mass, and radiation damping matrices. Then, the retardation function of the system is determined by inverse Fourier transform of the radiation damping matrix [37]. In this regard, note that the choice of adopting identical U-OWC chambers allowed reducing the computational cost of the semi-analytical computation because the resulting matrices are Toeplitz [38].

Given the retardation function matrix, the parameters of the Prony expansion, Eq. (2), can be identified. The procedure described by Roessling and Ringwood [32] has been used for determining the Prony parameters, but the numerical results showed that several terms in the Prony expansion were necessary for approximating accurately the retardation function components. Thus, the results of this method have been enhanced by an algorithm seeking the optimal Prony parameters via minimization of the mean square error between the target retardation function and the estimated one. For this purpose, the initial guess was obtained by the method in Roessling and Ringwood [32]. Then, the Python Scipy optimization tool has been used [39], where bounds on the Prony parameters have been established. Specifically, the parameters have been selected by ensuring that $\alpha_{ijm} \geq 0$, $-\infty < \beta_{ijm} < +\infty$, $\omega_{ijm} \geq 0$, and $-\pi < \phi_{ijm} \leq \pi$. For instance, consider the case of a U-OWC wave farm comprising nine converters. Figure 5 compares the retardation function element $K_{1,1}(t)$ computed by the standard identification procedure (left panel) with the one involving a further mean square error minimization procedure (right panel). It is seen that an excellent agreement can be achieved by utilizing only three terms of the Prony approximation, whereas the standard identification procedure barely captures the salient features of the function. Pertinent numerical analyses showed that this identification procedure allows representing the diagonal elements of the retardation function matrix with a rather small number of terms. However, more terms are needed for approximating with a similar level of accuracy the out-of-diagonal elements. This fact can be observed in Fig. 6, where three terms in the Prony expansion do not allow capturing the retardation function ($K_{1,9}(t)$) behavior after 10 s. This is due to the specific retardation function pattern. Indeed, fluctuations moving away from the simple damped harmonic behavior are less likely to be well approximated by few terms. Generally, including more terms in the expansion allows achieving better accuracy. In this regard, Fig. 7 shows that 10 terms approximate better the target function. Clearly, this fact might reduce the computational efficiency of the proposed procedure if several terms are needed for capturing well the overall retardation function matrix behavior. However, note that the computed radiation force values are largely dominated by the diagonal elements, while the relevance of the out-of-diagonal elements becomes rapidly negligible. Therefore, it may be argued that an excellent approximation of the near-to-diagonal elements is sufficient for estimating reliably the wave farm response.

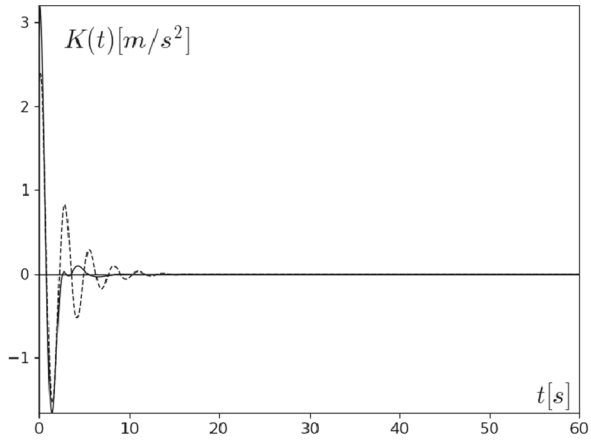


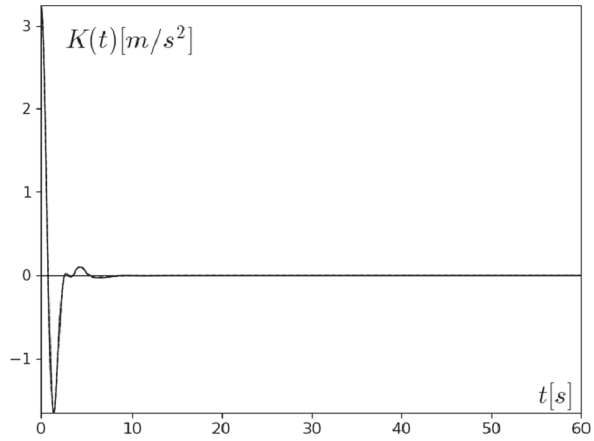


**Fig. 5** Diagonal element of the retardation function matrix pertaining to an array comprising 9 U-OWCs. Continuous line: target function. Dotted line: Prony approximation of order 3. Left panel: identification via the method described by Roessling and Ringwood [32]. Right panel: identification via mean square error minimization

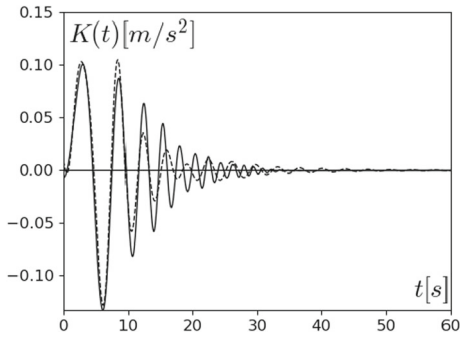


**Fig. 6** Element (1, 9) of the retardation function matrix pertaining to an array comprising 9 U-OWCs. Continuous line: target function. Dotted line: Prony approximation of order 3

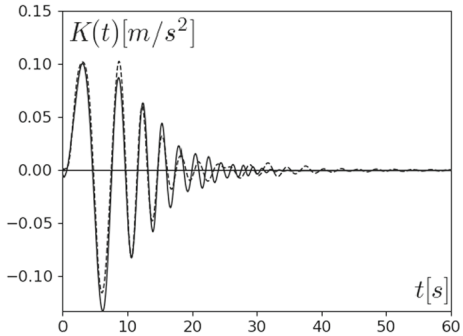


**Fig. 7** Element (1, 9) of the retardation function matrix pertaining to an array comprising 9 U-OWCs. Continuous line: target function. Dotted line: Prony approximation of order 10

The U-OWC dynamic model considered in this section was developed by Malara and Arena [36]. In such a model, the wave field in front of the wave farm is described by the potential flow theory, while the water column dynamics is described by the real fluid flow theory. Specifically, the water column equation of motion is governed by the unsteady Bernoulli equation [40] and the air pocket thermodynamic process is described by the conservation of mass principle in conjunction with the assumption of isentropic thermodynamic process [2]. In this regard, note that each of the air chambers is associated with one water column, and is assumed independent. Thus, there are no air mass exchanges between contiguous chambers. In this manner, the related governing equations are individually paired to the unsteady Bernoulli equations. In this context, the governing equations are

$$\begin{aligned}&\boldsymbol{M}(\boldsymbol{x})\,\ddot{\boldsymbol{x}}+\boldsymbol{C}(\boldsymbol{x},\dot{\boldsymbol{x}})\dot{\boldsymbol{x}}+\int_{-\infty}^{t}\boldsymbol{K}(t-\tau)\dot{\boldsymbol{x}}(\tau)d\tau+\boldsymbol{x}\\&\quad+\frac{1}{\rho g}(\boldsymbol{p}_c-p_{\text{atm}})\\&\quad=\frac{1}{\rho g}\Delta\boldsymbol{p}^{(D)}\end{aligned}\tag{47}$$

for the water column oscillations; and

$$\begin{aligned}&b_{2,i}b_{3,i}\big(h_{c,i}-x_i\big)\dot{p}_{c,i}-\gamma b_{2,i}b_{3,i}\dot{x}_i p_c\\&\quad+\gamma p_{c,i}\left(\frac{p_{\text{atm}}}{p_{c,i}}\right)^{\frac{1}{\gamma}}\frac{\dot{m}_{\text{turb},i}}{\rho_{\text{atm}}}\\&\quad=0,\ \text{for } i=1,\ldots,N_c,\end{aligned}\tag{48}$$

for each air chamber. The constants $g$, $\rho$, $\rho_{\text{atm}}$, $p_{\text{atm}}$, and $\gamma$ denote acceleration due to gravity; water density; atmospheric density; atmospheric pressure; and ratio between the specific heat at constant pressure and the

specific heat at constant volume, respectively. The system excitation $\Delta \boldsymbol{p}^{(D)}$ is the wave pressure computed at the U-OWC inlets in a diffracted wave field. The symbol $\dot{m}_{\text{turb},i}$ denotes the air mass flow rate through the turbines. This quantity is dependent upon the specific turbine under examination. In the case of Wells turbines, this is a linear function of the air chamber pressure. However, other models, such as the biradial turbine, are described by nonlinear relations with the air pressure [2]. Equations (47) and (48) are the coupled integro-differential equations governing the motion of a U-OWC wave farm. In this model, each U-OWC is described by water column displacement ($x_i$) and air pressure terms ($p_{c,i}$), which are captured by the vectors $\boldsymbol{x}$ and $\boldsymbol{p}_c$. Therefore, a wave farm comprising $N_c$ U-OWC converters has $2N_c$ degrees of freedom. However, the radiation term appears only in Eq. (47). This is due to the fact that the unsteady Bernoulli equation is derived by enforcing an energy balance between each U-OWC inlet and its associated water column free surface. So that, the radiated term arises from the representation of the water pressure at the U-OWC inlet via the Cummins' representation. In this regard, note that the units associated with these quantities are not the one commonly utilized in WEC models based on force equilibrium. Nevertheless, the mathematical formulation of the model studied herein can be treated by the numerical procedure described in the previous sections without a particular adjustment. Additional notable features of this model are: the inclusion of nonlinear mass terms, which account for the water mass variations occurring into the water column during the alternate crossing of wave crests and troughs; and the nonlinear damping terms due to the kinetic heads and to the head losses included into the computation of the total heads. In this regard, the expressions given by Malara and Arena [36] are used. That is,

$$\boldsymbol{M}(\boldsymbol{x}) = \frac{1+C_{in}}{g} \begin{bmatrix} \frac{b_{2,1}}{b_1} l_1 + l_1 + h + x_1 & 0 & 0 \\ 0 & \ddots & 0 \\ 0 & 0 & \frac{b_{2,N_c}}{b_1} l_{N_c} + l_{N_c} + h + x_{N_c} \end{bmatrix} + \boldsymbol{M}^{(\infty)}, \tag{49}$$

and $\boldsymbol{C}(\boldsymbol{x}, \dot{\boldsymbol{x}})$ is a diagonal matrix with elements,

$$\{\boldsymbol{C}(\boldsymbol{x}, \dot{\boldsymbol{x}})\}_{ii} = \frac{1}{2g} \left\{ C_{dg} \left[ \frac{l_i}{R_{h1,i}} \left( \frac{b_{2,i}}{b_1} \right)^2 + \frac{l_i + h + x_i}{R_{h2,i}} \right] |\dot{x}_i| + \left( 1 - \frac{b_{2,i}^2}{b_1^2} \right) \dot{x}_i \right\}, \; for \; i = 1, \ldots, N_c. \tag{50}$$

The coefficients $C_{in}$ and $C_{dg}$ are empirical coefficients accounting for experimentally observed head losses. In the numerical calculations, they are set equal to 0.13 and 0.71, respectively [41]. Further, $R_{h1,i}$ and $R_{h2,i}$ denote the hydraulic radii of the U-ducts and of the inner chambers, respectively.

The turbine model incorporated in Eq. (48) is the Wells turbine [42]. The air flow rate of this turbine depends linearly on the air chamber pressure drop. That is,

$$\dot{m}_{\text{turb},i} = \frac{\Lambda_i D_i}{\varpi_i} \left( p_{c,i} - p_{\text{atm}} \right), \tag{51}$$

where $\Lambda_i$ is a turbine characteristic parameter, and $\varpi_i$ is the turbine rotational speed. In the proposed numerical computations, identical turbine models working at a constant rotational speed are considered. Specifically, the turbine coefficient $\Lambda_i$ is set equal to 0.3 and the rotational speed is $\varpi = 2800$ rpm. These parameters have been already utilized for similar U-OWC plants [43].

Given the wave farm response, the overall farm power output can be determined. For this purpose, the following equation is used for computing the instantaneous pneumatic power available to the turbine:

$$P_i(t) = \left( p_{c,i} - p_{\text{atm}} \right) \frac{\dot{m}_{\text{turb},i}}{\rho_{\text{atm}}} \tag{52}$$

Obviously, the average pneumatic power available to the turbine over a time span $T$ is

$$P_{m,i} = \frac{1}{T} \int_0^T P_i(t) dt. \tag{53}$$

#### 4.2.1 *Reliability: response to harmonic wave excitation case*

Next the reliability of the proposed numerical procedure for computing the radiation force is assessed. Specifically, the response of U-OWCs exposed to deterministic linear sea waves is computed by the

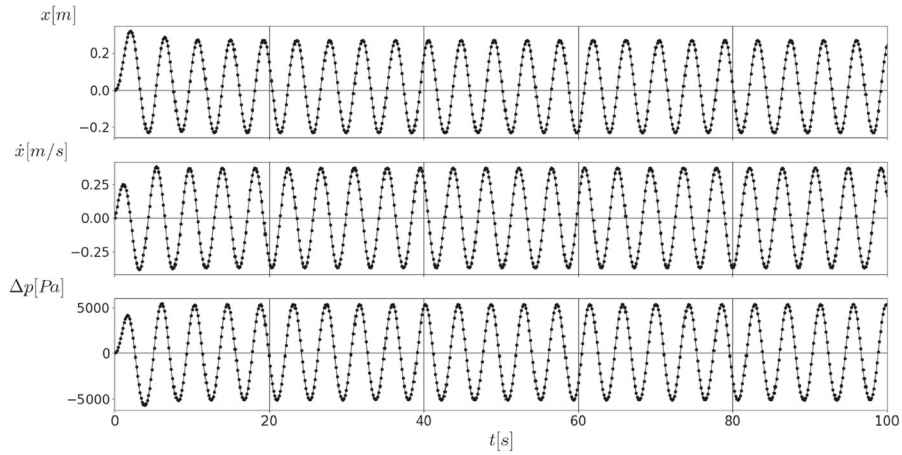


**Fig. 8** Time domain response of a U-OWC with 1 chamber. Top panel: water column displacement. Central panel: water column velocity. Lower panel: air chamber pressure drop. Continuous lines: computation via trapezoidal approximation of the convolution integral. Circles: computation via Prony expansion with three terms

proposed approach and by a classical Newmark scheme in which the convolution integrals are computed by the trapezoidal rule. All numerical examples involve regular incident waves having wave height $H = 1$ m, period $T = 4.26$ s, and direction of propagation orthogonal to the U-OWC layout. The U-OWC responses are computed over a time span of 100 s, with a constant time step $\Delta t = 0.01$ s and directly compared in time domain.

The first comparison considers the basic problem of an isolated U-OWC exposed to regular waves. In this context, the system involves two degrees of freedom and three state variables: the water column displacement $x$, the water column velocity $\dot{x}$, and the air chamber pressure drop $\Delta p = p_c - p_{atm}$. Figure 8 shows the results obtained by the classical numerical integration based on the trapezoidal rule (continuous lines), and the ones obtained by the proposed approach (circles). It is seen that the proposed approach provides an excellent estimation of all of the response components. Further, it is capable of estimating perfectly also the transient part of the response, where larger fluctuations of the components can be observed. In this context, note that this accuracy is obtained by utilizing three terms of the Prony expansion.

Next, the algorithm is tested by considering a wave farm comprising 9 U-OWCs. In this context, the farm is a system described by 18 degrees of freedom. Even in this case, the proposed approach is implemented by retaining only three terms in the Prony expansion. Figures 9 and 10 compare the farm response components associated with the extremal chamber of the

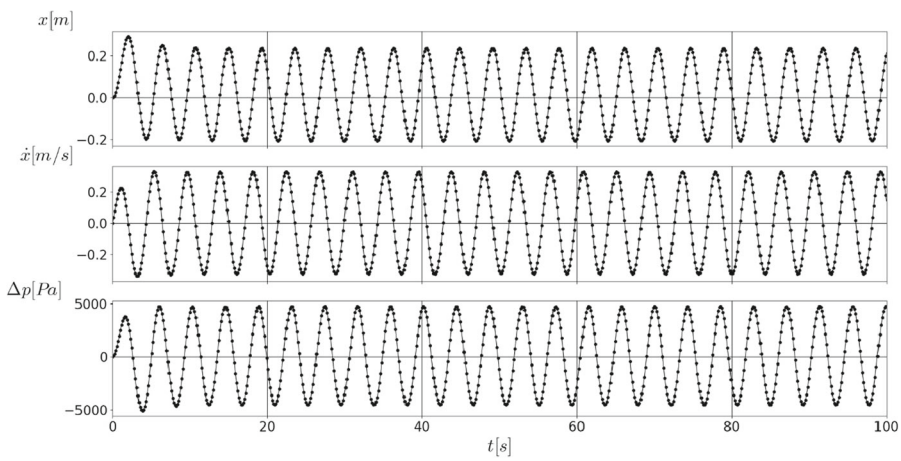


**Fig. 9** Time domain response of the extremal chamber of an array comprising nine chambers. Top panel: water column displacement. Central panel: water column velocity. Lower panel: air chamber pressure drop. Continuous lines: computation via trapezoidal approximation of the convolution integral. Circles: computation via Prony expansion with three terms

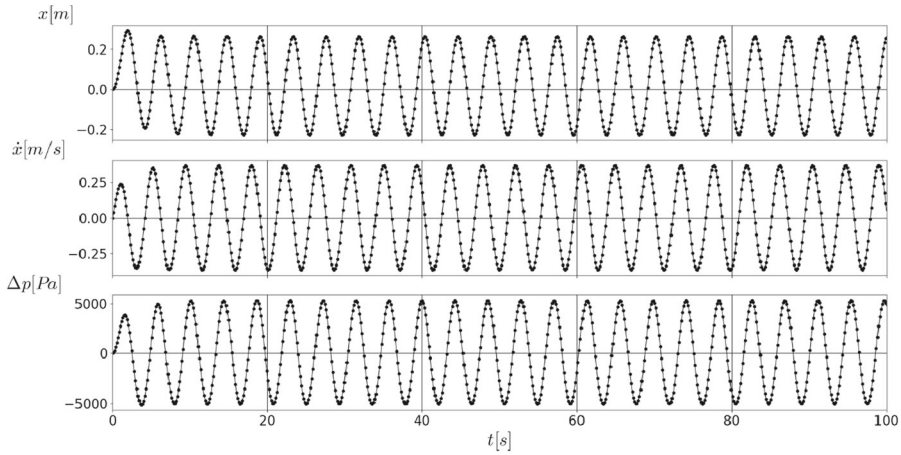


**Fig. 10** Time domain response of the central chamber of an array comprising nine chambers. Top panel: water column displacement. Central panel: water column velocity. Lower panel: air chamber pressure drop. Continuous lines: computation via trapezoidal approximation of the convolution integral. Circles: computation via Prony expansion with three terms

array, and with the central chamber of the array, respectively. It is seen that all response components are estimated quite reliably over the entire time domain in all chambers. In this case, note that this level of accuracy is obtained despite the use of only three terms of the Prony expansion. Indeed, the previous section showed that such a small number of terms does not allow capturing the retardation function pattern associated with the out-of-diagonal elements of the retardation function matrix. However, the fact that the overall wave farm dynamics is mostly influenced by the diagonal (or near-to-diagonal) elements allows obtaining quite reliable estimates using an excellent approximation of just these elements.

#### 4.2.2 *Efficiency: response to random wave excitation case*

Next, the efficiency of the proposed approach is examined in the context of computationally costly Monte Carlo simulations. Monte Carlo data are produced for assessing, by numerical methods, the behavior of the wave farm in realistic conditions, and determining the response statistics (means, variances, average power outputs, etc.). Monte Carlo simulations are characterized by costly running times due to the fact that reliable estimates of the response statistics can be obtained only using an adequately large number of response samples. In wave energy applications, this computational barrier is partially limited by the fact that sea waves are described as ergodic Gaussian random processes with a known spectrum [44]. Therefore, relevant response statistics are determined from one realization of the response by exploiting the ergodicity assumption. However, if the wave farm is exposed to non-stationary excitations (such as earthquake excitations) multiple realizations of response are needed [17]. In this context, traditional methods can be utilized requiring, however, high performance computational hardware, but for the case of massive wave power farms the cost may be prohibitive.

The following numerical results are obtained by synthesizing spectrum compatible realizations of the wave farm excitation. For this purpose, the incident wave field is made compatible with a mean JONSWAP frequency spectrum with Mitsuyasu directional spreading function [45, 46], in which the significant wave height $H_s = 1.5$ m and the peak spectral period $T_p = 5.22$ s. For determining response statistics and average power outputs, $10^6$ samples of the response components are calculated per realization by adopting a time step $\Delta t = 0.01$ s over a simulation time of 10.000 s. The numerical simulations are executed for wave power farms having $N = 1, 7, 15, 31$ U-OWCs (therefore 2, 14, 30, 62 degrees of freedom). In all cases, the response statistics pertaining to the central U-OWC of the wave farm are shown. Figure 11 shows a comparison between the statistics obtained by the proposed Prony-based method (circles) and the classical trapezoidal integration (crosses). The figure compares the standard deviations of the response components (displacement and air pressure drop) and the average power available to the turbine. Consistently with the observations pertaining to the harmonic wave excitation case, the response statistics

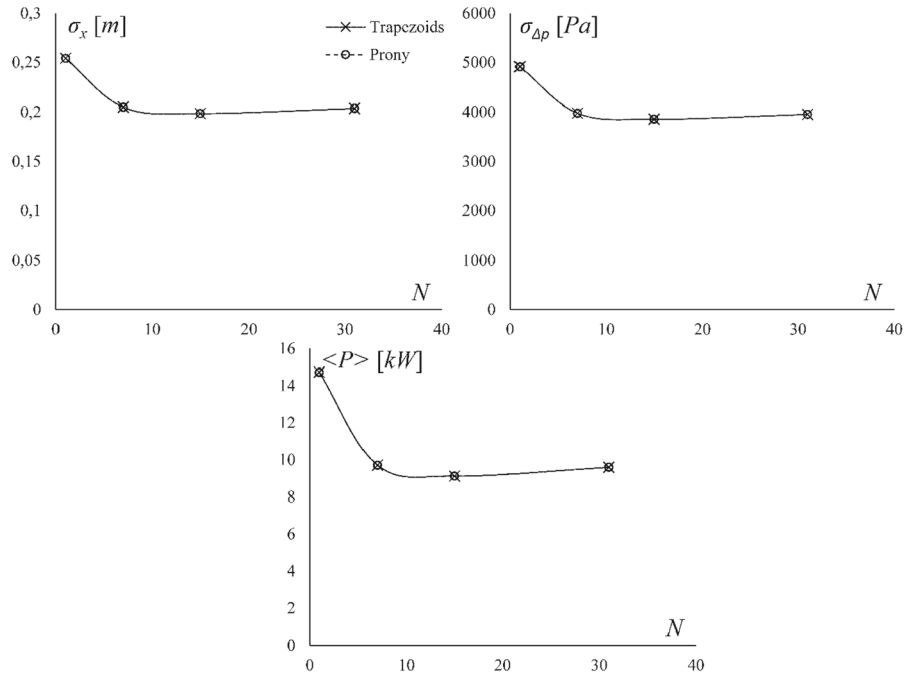


**Fig. 11** Standard deviations of displacement ($\sigma_x$) and air pressure drop ($\sigma_{\Delta p}$) and average power available to the turbine of the central chamber of a U-OWC farm with $N$ converters

are estimated perfectly by the proposed method irrespective of the size of the wave power farm. Note that this level of accuracy is obtained by approximating the retardation function matrix elements just by three terms in the Prony expansion.

The efficiency of the proposed method is assessed by running time comparisons. For this purpose, the time required by the computational hardware for integrating the equation of motion over the entire time span is recorded. This time does not include the time spent for synthesizing the wave farm excitation and the data post-processing. For producing comparable data, the proposed and the classical integration methods are coded both in Python language and executed in a Windows environment using an Intel® Xeon® CPU E5-2690 @ 2.90 GHz with 64 GB of installed RAM. The results discussed in this numerical section have not been obtained by accelerated GPU computations and have not taken advantage of code parallelization. Instead, the numerical execution of the code has been accelerated software—wise by executing the numerical solver through the Numba just-in-time compiler [47].

Figure 12 compares the running time of the integration by trapezoid vis-à-vis the running time of the Prony-based integration. It is seen that the proposed approach is significantly more efficient than the classical one. In this regard, note that the vertical axis of the figure is in logarithmic scale. While comparable results are obtained in case of a single U-OWC, a marked difference arises in the scenario of gradually increasing farms. The great efficiency of the proposed approach over the conventional one is quite evident by considering a farm comprising 31 U-OWCs (therefore 62 degrees of freedom). In this case, the standard approach requires a computational time of about

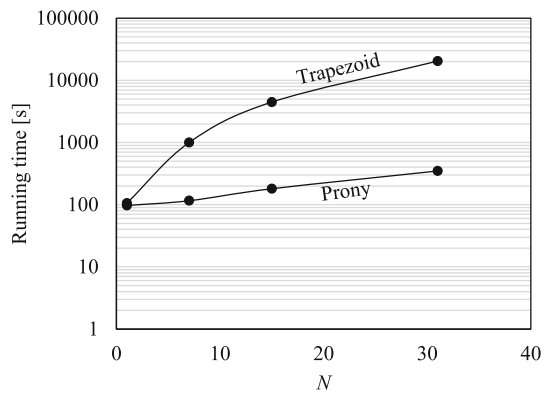


**Fig. 12** Running time versus number of WECs. Direct integration through trapezoids vis-à-vis integration through Prony expansion

20,000 s ($\sim$ 5, 5 h), while the proposed approach requires 348 s.

## 5 Concluding remarks

This paper has dealt with the problem of efficient computation of the wave power farm response in the time domain. Specifically, it has proposed a numerical approach for computing efficiently the radiation force typically included in wave energy converter models described via the Cummins' equation.

The approach is based on the approximation of the retardation function matrix elements via the Prony method. This allows computing, through a novel scheme, recursively the convolution integrals associated with the radiation forces at each time instant from their known previous values. Compared to other approaches available in the open literature, this approach does not require storing past response values (as required by the direct computation of the convolution integral), and does not augment the number of the differential equations governing the wave farm dynamics (as done in standard state-space approaches).

The reliability and efficiency of the algorithm have been shown by comparisons in the time domain, and by measuring the running times of the algorithm. It has been found that the algorithm determines quite reliably both the stationary and the transient parts of the wave farm response irrespective of the wave farm size. In the context of Monte Carlo simulation studies, the algorithm significantly reduces the computational costs. In this regard, it is mentioned that it was capable to yield farm response parameters in 350 s versus the 5.5 h required by a straightforward numerical integration of the equation of motion.

Clearly, the technique proposed in this article is not limited to wave energy-related applications. Indeed, it can be applied to any problem of dynamics governed by integro-differential equations, in which the elements of the convolution integral matrix kernel can be approximated reliably by the Prony method.

**Acknowledgements** Felice Arena and Giovanni Malara acknowledge the partial support of Italian Ministry of Infrastructures and Sustainable Mobility through the project "Green Campania Ports" funded by the "Programma di azione e coesione "INFRASTRUTTURE E RETI" 2014–2020".

**Funding** Open access funding provided by Università degli Studi Mediterranea di Reggio Calabria within the CRUI-CARE Agreement.

**Data availability** The datasets generated and/or analyzed during the current study are available from the corresponding author on reasonable request.

**Declarations**

**Conflict of interest** The authors have no conflict of interest.



## References

1. Guo, B., Wang, T., Jin, S., Duan, S., Yang, K., Zhao, Y.: A review of point absorber wave energy converters. J. Marine Sci. Eng. **10**, 1534 (2022). https://doi.org/10.3390/JMSE10101534
2. Falcão, A.F.O., Henriques, J.C.C.: Oscillating-water-column wave energy converters and air turbines: a review. Renew. Energy **85**, 1391–1424 (2016). https://doi.org/10.1016/j.renene.2015.07.086
3. Palma, G., Contestabile, P., Zanuttigh, B., Formentin, S.M., Vicinanza, D.: Integrated assessment of the hydraulic and structural performance of the OBREC device in the Gulf of Naples Italy. Appl. Ocean Res. **101**, 102217 (2020). https://doi.org/10.1016/j.apor.2020.102217
4. Draycott, S., Szadkowska, I., Silva, M., Ingram, D.M.: Assessing the macro-economic benefit of installing a farm of oscillating water columns in Scotland And Portugal. Energies **11**, 2824 (2018). https://doi.org/10.3390/EN11102824
5. IRENA: Renewable Power Generation Costs in 2019. International Renewable Energy Agency, Abu Dhabi (2020)
6. Purvins, A., Zubaryeva, A., Llorente, M., Tzimas, E., Mercier, A.: Challenges and options for a large wind power uptake by the European electricity system. Appl. Energy **88**, 1461–1469 (2011). https://doi.org/10.1016/J.APENERGY.2010.12.017
7. Garcia-Rosa, P.B., Bacelli, G., Ringwood, J.V.: Control-informed optimal array layout for wave farms. IEEE Trans. Sustain. Energy **6**, 575–582 (2015). https://doi.org/10.1109/TSTE.2015.2394750

8. Child, B.F.M., Venugopal, V.: Optimal configurations of wave energy device arrays. Ocean Eng. **37**, 1402–1417 (2010). https://doi.org/10.1016/J.OCEANENG.2010.06.010
9. Yang, B., Wu, S., Zhang, H., Liu, B., Shu, H., Shan, J., Ren, Y., Yao, W.: Wave energy converter array layout optimization: a critical and comprehensive overview. Renew. Sustain. Energy Rev. **167**, 112668 (2022). https://doi.org/10.1016/J.RSER.2022.112668
10. Mei, C.C., Stiassnie, M., Yue, D.K.K.: Theory and applications of ocean surface waves. World Scientific, Singapore (2005)
11. Cummins, W.E.: The impulse response function and ship motions. Schiffstechnik **1962**(57), 101–109 (1962). https://doi.org/10.1179/2056711115Y.00000000001
12. Sarkar, D., Contal, E., Vayatis, N., Dias, F.: Prediction and optimization of wave energy converter arrays using a machine learning approach. Renew. Energy **97**, 504–517 (2016). https://doi.org/10.1016/J.RENENE.2016.05.083
13. Giassi, M., Thomas, S., Tosdevin, T., Engström, J., Hann, M., Isberg, J., Göteman, M.: Capturing the experimental behaviour of a point-absorber WEC by simplified numerical models. J. Fluids Struct. **99**, 103143 (2020). https://doi.org/10.1016/J.JFLUIDSTRUCTS.2020.103143
14. Falcão, A.F.O., Rodrigues, R.J.A.: Stochastic modelling of OWC wave power plant performance. Appl. Ocean Res. **24**, 59–71 (2002). https://doi.org/10.1016/S0141-1187(02)00022-6
15. Righi, M., Moretti, G., Forehand, D., Agostini, L., Vertechy, R., Fontana, M.: A broadbanded pressure differential wave energy converter based on dielectric elastomer generators. Nonlinear Dyn. **105**, 2861–2876 (2021). https://doi.org/10.1007/s11071-021-06721-8
16. Rosati Papini, G., Pietro Moretti, G., Vertechy, R., Fontana, M.: Control of an oscillating water column wave energy converter based on dielectric elastomer generator. Nonlinear Dyn. **92**, 181–202 (2018). https://doi.org/10.1007/s11071-018-4048-x
17. Roberts, J.B., Spanos, P.D.: Random Vibration and Statistical Linearization. Dover Publications, Mineola, New York, USA (2003)
18. Malara, G., Spanos, P.D.: Efficient determination of nonlinear response of an array of oscillating water column energy harvesters exposed to random sea waves. Nonlinear Dyn. **98**, 2019–2034 (2019). https://doi.org/10.1007/s11071-019-05303-z
19. Silva, L.S.P., Sergiienko, N.Y., Pesce, C.P., Ding, B., Cazzolato, B., Morishita, H.M.: Stochastic analysis of nonlinear wave energy converters via statistical linearization. Appl. Ocean Res. **95**, 102023 (2020). https://doi.org/10.1016/J.APOR.2019.102023
20. Spanos, P.D., Arena, F., Richichi, A., Malara, G.: Efficient dynamic analysis of a nonlinear wave energy harvester model. J. Offshore Mech. Arct. Eng. **138**, 041901 (2016). https://doi.org/10.1115/1.4032898
21. Faedo, N., Giorgi, G., Ringwood, J.V., Mattiazzo, G.: Optimal control of wave energy systems considering nonlinear Froude–Krylov effects: control-oriented modelling and moment-based control. Nonlinear Dyn. **109**, 1777–1804 (2022). https://doi.org/10.1007/s11071-022-07530-3
22. Faedo, N., Dores Piuma, F.J., Giorgi, G., Ringwood, J.V.: Nonlinear model reduction for wave energy systems: a moment-matching-based approach. Nonlinear Dyn. **102**, 1215–1237 (2020). https://doi.org/10.1007/s11071-020-06028-0
23. Yu, Z., Falnes, J.: State-space modelling of a vertical cylinder in heave. Appl. Ocean Res. **17**, 265–275 (1995). https://doi.org/10.1016/0141-1187(96)00002-8
24. Stavropoulou, C., Goude, A., Katsidoniotaki, E., Göteman, M.: Fast time-domain model for the preliminary design of a wave power farm. Renew. Energy **219**, 119482 (2023). https://doi.org/10.1016/J.RENENE.2023.119482
25. Slyusar, V.I.: Interpretation of the Proni method for solving long-range problems. Radioelectron. Commun. Syst. **41**, 35–39 (1998)
26. Henriques, J.C.C., Portillo, J.C.C., Sheng, W., Gato, L.M.C., Falcão, A.F.O.: Dynamics and control of air turbines in oscillating-water-column wave energy converters: analyses and case study. Renew. Sustain. Energy Rev. **112**, 571–589 (2019). https://doi.org/10.1016/J.RSER.2019.05.010
27. Faedo, N., Peña-Sanchez, Y., Ringwood, J.V.: Parameterisation of Radiation forces for multiple degree-of-freedom wave energy converters using moment-matching. Int. J. Offshore Polar Eng. **30**, 395–402 (2020). https://doi.org/10.17736/IJOPE.2020.MK71
28. Newman, J.N., Malenica, S., Ouled Housseine, C.: Added mass and damping of structures with periodic angular shape. J. Fluid Mech. **948**, R1 (2022). https://doi.org/10.1017/JFM.2022.709
29. Kurnia, R., Ducrozet, G.: NEMOH: Open-source boundary element solver for computation of first- and second-order hydrodynamic loads in the frequency domain. Comput. Phys. Commun. **292**, 108885 (2023). https://doi.org/10.1016/J.CPC.2023.108885
30. Göteman, M., Engström, J., Eriksson, M., Isberg, J.: Fast modeling of large wave energy farms using interaction distance cut-off. Energies **8**, 13741–13757 (2015). https://doi.org/10.3390/EN81212394
31. Pereyra, V., Scherer, G.: Exponential data fitting. In: Exponential Data Fitting and its Applications, pp. 1–26. Bentham Science Publishers Ltd, Sharjah (2010)
32. Roessling, A., Ringwood, J.V.: Finite order approximations to radiation forces for wave energy applications. Renewable energies offshore. **359**, 359–366 (2015)
33. Clough, R.W., Penzien, J.: Dynamics of structures. Computers & Structures Inc, Berkeley, CA, USA (1995)
34. Arena, F., Romolo, A., Malara, G., Ascanelli, A.: On Design and Building of a U-OWC Wave Energy Converter in the Mediterranean Sea: A Case Study. In: Proc. of the 32nd International Conference on Ocean, Offshore and Arctic Engineering. p. V008T09A102. Nantes, France (2013)
35. Arena, F., Romolo, A., Ascanelli, A., Ferrante, A., Ghiretti, S., Valentino, E.: Green ports: an Italian experience. In: IV Congreso Nacional de la Asociación Técnica de Puertos y Costas. pp. 391–405. Valencia, Spain (2012)
36. Malara, G., Arena, F.: Response of U-oscillating water column arrays: semi-analytical approach and numerical results. Renew. Energy **138**, 1152–1165 (2019). https://doi.org/10.1016/j.renene.2019.02.018

37. Falnes, J.: Ocean waves and oscillating systems: linear interactions including wave-energy extraction. Cambridge University Press, Cambridge, UK (2004)
38. Gray, R.M.: Toeplitz and Circulant matrices: a review. foundations and trends®. Commun. Inf. Theory **2**, 155–239 (2005). https://doi.org/10.1561/0100000006
39. Virtanen, P., Gommers, R., Oliphant, T.E., Haberland, M., Reddy, T., Cournapeau, D., Burovski, E., Peterson, P., Weckesser, W., Bright, J., van der Walt, S.J., Brett, M., Wilson, J., Millman, K.J., Mayorov, N., Nelson, A.R.J., Jones, E., Kern, R., Larson, E., Carey, C.J., Polat, İ, Feng, Y., Moore, E.W., VanderPlas, J., Laxalde, D., Perktold, J., Cimrman, R., Henriksen, I., Quintero, E.A., Harris, C.R., Archibald, A.M., Ribeiro, A.H., Pedregosa, F., van Mulbregt, P., Vijaykumar, A., Bardelli, A.P., Rothberg, A., Hilboll, A., Kloeckner, A., Scopatz, A., Lee, A., Rokem, A., Woods, C.N., Fulton, C., Masson, C., Häggström, C., Fitzgerald, C., Nicholson, D.A., Hagen, D.R., Pasechnik, D.V., Olivetti, E., Martin, E., Wieser, E., Silva, F., Lenders, F., Wilhelm, F., Young, G., Price, G.A., Ingold, G.L., Allen, G.E., Lee, G.R., Audren, H., Probst, I., Dietrich, J.P., Silterra, J., Webber, J.T., Slavič, J., Nothman, J., Buchner, J., Kulick, J., Schönberger, J.L., de Miranda Cardoso, J.V., Reimer, J., Harrington, J., Rodríguez, J.L.C., Nunez-Iglesias, J., Kuczynski, J., Tritz, K., Thoma, M., Newville, M., Kümmerer, M., Bolingbroke, M., Tartre, M., Pak, M., Smith, N.J., Nowaczyk, N., Shebanov, N., Pavlyk, O., Brodtkorb, P.A., Lee, P., McGibbon, R.T., Feldbauer, R., Lewis, S., Tygier, S., Sievert, S., Vigna, S., Peterson, S., More, S., Pudlik, T., Oshima, T., Pingel, T.J., Robitaille, T.P., Spura, T., Jones, T.R., Cera, T., Leslie, T., Zito, T., Krauss, T., Upadhyay, U., Halchenko, Y.O., Vázquez-Baeza, Y.: SciPy 1.0: fundamental algorithms for scientific computing in python. Nat. Methods **17**, 261–272 (2020). https://doi.org/10.1038/s41592-019-0686-2
40. Batchelor, G.K.: An introduction to fluid dynamics. Cambridge University Press, Cambridge, UK (2000)
41. Malara, G., Romolo, A., Fiamma, V., Arena, F.: On the modelling of water column oscillations in U-OWC energy harvesters. Renew. Energy **101**, 964–972 (2017). https://doi.org/10.1016/j.renene.2016.09.051
42. Wells, A.A.: Fluid Driven Rotary Transducer, (1976)
43. Scialò, A., Henriques, J.C.C., Malara, G., Falcão, A.F.O., Gato, L.M.C., Arena, F.: Power take-off selection for a fixed U-OWC wave power plant in the Mediterranean sea: the case of Roccella Jonica. Energy **215**, 119085 (2021). https://doi.org/10.1016/j.energy.2020.119085
44. Ochi, M.K.: Ocean waves: the stochastic approach. Cambridge University Press, Cambridge, United Kingdom (2005)
45. Hasselmann, K., Barnett, T.P., Bouws, E., Carlson, H., Cartwright, D.E., Enke, K., Ewing, J.A., Gienapp, H., Hasselmann, D.E., Kruseman, P., Meerburg, A., Muller, P., Olbers, D.J., Richter, K., Sell, W., Walden, H.: Measurements of wind-wave growth and swell decay during the joint North sea wave project (JONSWAP). Ergnzungsheft zur Deutschen Hydrographischen Zeitschrift Reihe **A**(8), 95 (1973)
46. Mitsuyasu, H., Tasai, F., Suhara, T., Mizuno, S., Ohkusu, M., Honda, T., Rikiishi, K.: Observations of the directional spectrum of ocean wavesusing a cloverleaf buoy. J. Phys. Oceanogr. **5**, 750–760 (1975). https://doi.org/10.1175/1520-0485(1975)005%3c0750:OOTDSO%3e2.0.CO;2
47. Lam, S.K., Pitrou, A., Seibert, S.: Numba: A LLVM-based Python JIT Compiler. In: Proceedings of LLVM-HPC 2015: 2nd Workshop on the LLVM Compiler Infrastructure in HPC-held in conjunction with SC 2015: the international conference for high performance computing, networking, storage and analysis. 2015-Janua, (2015). https://doi.org/10.1145/2833157.2833162